Renewable Energy 71 (2014) 453–465

Contents lists available at ScienceDirect

Renewable Energy

journal homepage: www.elsevier.com/locate/renene

State estimation for wind farms including the wind turbine generator models

Blanca Nieves Miranda-Blanco, Eloy Díaz-Dorado, Camilo Carrillo*, J. Cidrás

University of Vigo, Spain

ARTICLE INFO

Article history:
Received 28 June 2013
Accepted 13 May 2014
Available online

Keywords:
Wind energy
State estimation
State estimation with constraints
Neural networks

ABSTRACT

Wind farms can be analyzed using state estimation methods, which can be used to obtain its running state, including several aspects that cannot be easily obtained using other methods (e.g., capacitor bank aging) Using these methods on these types of networks is strongly affected by decoupling between active and reactive power and by a radial configuration, which is typical. For example, this decoupling affects its observability and robustness as well as the technical feasibility of the results. To overcome these drawbacks, an extended state estimation method is proposed in which the models for the different wind turbine technologies have been incorporated. These models have been mainly generated from measurement data using neural networks and polynomial fitting; these models do not require parameter values, which are rarely available from manufacturers. Furthermore, the resulting equations for modeling wind turbines are easily integrated into the state estimator due to their simplicity and derivatives.Thus, a method that guarantees feasible results, at least for wind turbines, was generated with increased observability robustness.

The method was tested using measurement data from the Sotavento Wind Park, which has wind turbines with different types of technologies.

1. Introduction

The statuses of the network and wind turbine generators (WTGs) are useful for evaluating the proper working conditions of a wind park; the data from Supervisory Control and Data Acquisition (SCADA) can be used and are usually implemented in this type of installation. However, directly using measured data can generate errors associated with measurement errors and communication failures, among other concerns. Furthermore, it can only be obtained values directly calculated from measurements; thus, several relevant factors (e.g., capacitor aging) cannot usually be available. In this context, state estimation (SE) methods can overcome these problems.

State estimation (SE) is a method for obtaining the state variables of a network from a set of measurements [1,2]. Usually, the measurements are the active and reactive power flowing through the branches and injected at nodes as well as the magnitude of the nodes' voltage. Apart from obtaining the network state, this type of analysis could be useful for analyzing other aspects related to the system operation (e.g., out-of-service WTGs, aging capacitor banks, communication failures and energy loss estimates).

When an SE method is applied, it must be considered that a wind farm network is usually in a radial configuration, and the electrical measurements are only conducted on the low voltage side of the wind turbines (WTGs) and the high voltage side of the substation. Thus, the common measurements are the voltage at the nodes, the active and reactive power generated by the WTGs and the active and reactive power injected into the transmission network through the substation. A state estimator in this type of network has little redundancy because it only includes nodal measurements, and the active power (voltage angles) is strongly decoupled from the reactive power (voltage magnitudes). Therefore, the resulting system has a weak observability; this means that if the measurements in only one WTG are not available, then the system may not be observable. Furthermore, there is no guarantee that the results are technically feasible (e.g., due to out-of-range values, unrealistic power flows and values that are incompatible with WTG operation) because the WTG behavior (e.g., the PQ model of asynchronous machines) is not included in the method.

To overcome the aforementioned drawbacks, this paper proposes to include functions that model the WTG behavior (i.e.,

* Corresponding author. EEI – Sede Campus, Universidade de Vigo, Campus Universitario, 36310 Vigo, Spain. Tel.: +34 986813912.
E-mail addresses: blancan@uvigo.es (B.N. Miranda-Blanco), ediaz@uvigo.es (E. Díaz-Dorado), carrillo@uvigo.es (C. Carrillo), jcidras@uvigo.es (J. Cidrás).

http://dx.doi.org/10.1016/j.renene.2014.05.029
0960-1481/

Nomenclature

k	number of iterations
x	state vector (module U_i and θ_i nodal voltage phase)
h	functions that relate measurements to state variables
z^m	measurements vector
ε	errors vector
d	constraints vector
$c(x)$	functions of the constraints vector
W	inverse covariance matrix
H	Jacobian matrix of the functions $h(x)$, in $x^{(i)}$
C	constraint matrix
$\Delta z^{(i)}$	vector measurement errors z^m
P_i	active power injected at node i
Q_i	reactive power injected at node i
Q_{Ci}	reactive power generated by capacitors in node i
U_i^m	measurement of the voltage at node i
P_i^m	measurement of the active power injected at node i
Q_i^m	measurement of the reactive power injected at node i
Q_{Ci}^m	measurement of the reactive power generated by the capacitors in node i
n	number of nodes in the network
N	set of nodes in the system
nn_R	reference node for voltage angles
N_{Um}	set of nodes with voltage measurements
N_{Pm}	set of nodes with injected active power measurements
N_{Qm}	set of nodes with injected reactive power measurements
N_{null}	set of nodes with virtual measurements (null injected active and reactive power)
N_e	set of nodes with active and reactive power that belongs to the extended state vector
$N_{e,FSWT}$	set of nodes for FSWTs
$N_{e,VSWT-DFIGs}$	set of stator-side nodes in VSWT-DFIGs
$N_{e,VSWT-DFIGr}$	set of rotor-side nodes in VSWT-DFIGs
$N_{e,VSWT-SG}$	set of nodes for VSWT-SGs
$X_{(N)}^m$	vector of measurements X_i^m at nodes N; thus, $X_{(N)}^m = [\ldots \quad X_i^m \quad \ldots] \quad i \in N$

functions that establish the relationship between voltage, active power and reactive power in WTGs) in the state estimation equations. These relationships are not usually included in a classic state estimation [3]; they are only partially considered in certain power flow analyses [4,5,6].

To model WTGs, equations can be used that typically include the slip as input data and several assumptions about the generator behavior (e.g., the relationship between power and slip) [7,8]. Using these equations has certain disadvantages: the need for slip measurements; the equation parameters are usually unknown; and finally, the additional complexity in the state estimator does not guarantee enhanced redundancy.

To overcome those problems, herein, WTGs were modeled using polynomial fitting techniques and *back-propagation neural networks* (*BPNNs*) [9,10]. Thus, the input data for the proposed state estimator are the network parameters and measurements; the latter are used for WTG modeling and during SE. The resulting models, polynomial equations and BPNNs can easily be integrated into the SE due to their simplicity and derivatives. To integrate these functions into the state estimator, a method is proposed that increases the number of state variables, including the variables active and reactive power of wind turbines, and uses the WTG models as restrictions. As a result, the state estimation problem becomes a constrained optimization problem [11,12]. The main advantage of the proposed model is that the decoupling between P–V and between Q-δ disappears, the system redundancy is increased, and the results obtained are technically feasible due to inclusion of the WTG models.

To demonstrate its operation, the proposed method was applied to the Sotavento Experimental Wind Farm S.A. (http://www.sotaventogalicia.com) [13,14]. This farm is dedicated to D&I of wind power and includes nine different types of 24 WTGs, including fixed-speed and variable-speed wind turbines.

2. Static state estimation

2.1. Classical state estimator

Static state estimation (SE) consists of calculating a set of variables (state variables) from a set of network measurements. Usually, the measurements are at the magnitude of the node voltages, the active and reactive power flow in branches and the active and reactive power injection in nodes. On the other hand, the state variables are the magnitude and angle of the node voltages. When the state variables are known, any electric variable in any element of the network can be obtained. A diagram of the classical SE methodology is shown in Fig. 1.

In SE, the measurements are considered erroneous with the following behavior:

1. The histogram of the error values can be approximated using a normal pdf with the mean μ and standard deviation σ: $N(\mu,\sigma)$.
2. The expectation of errors is zero: $E[e_i] = 0$.
3. The errors are independent: $E[e_i \cdot e_j] = 0$; thus, it can be defined as a diagonal covariance matrix, where the main diagonal is the standard deviation vector:

$$Cov(e) = E\left[e \cdot e^T\right] = W^{-1} = diag\left\{\sigma_1^2, \sigma_2^2, \ldots, \sigma_m^2\right\}. \tag{1}$$

The SE method consists of calculating the state vector x such that the error between the measured values and those obtained from the estimator is minimized. According to previous paragraphs, assuming that measurements have an associated error (ε), the following system of equations can be written [1]:

$$z^m = h(x) + \varepsilon. \tag{2}$$

Therefore, the following index must be minimized [10]:

$$\min\{J(x)\} = \min\left\{[z - h(x)]^T \cdot W \cdot [z - h(x)]\right\}. \tag{3}$$

The method to minimize this term is the weighted least squares method. The state vector can be obtained by iteratively solving the following system of equations:

$$\left(H^T\left(x^{(k)}\right) \cdot W \cdot H\left(x^{(k)}\right)\right) \cdot \Delta x^{(k)} = H^T\left(x^{(k)}\right) \cdot W \cdot \left(\Delta z^{(k)}\right)$$
$$x^{(k+1)} = x^{(k)} + \Delta x^{(k)} \tag{4}$$

$$\Delta z^{(k)} = z^m - h\left(x^{(k)}\right). \tag{5}$$

For a wind farm, the state vector is formed by the angle of voltage at every network node except the reference node n_R and the

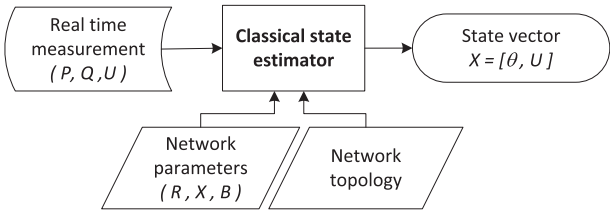

Fig. 1. Implementation methodology for a classical state estimator.

magnitude voltage at every network node, which yields the following:

$$x = \left[\theta_{(\mathcal{N}-n_R)} \quad U_{(\mathcal{N})}\right]. \tag{6}$$

The measurement vector is formed by the entire available voltage magnitude as well as the active power and reactive power values, including the interconnection nodes with a null P and Q. The resulting measurement vector can be written as follows:

$$z^m = \left[U^m_{(\mathcal{N}_{\mathrm{Um}})} \quad P^m_{(\mathcal{N}_{\mathrm{Pm}})} \quad P^m_{(\mathcal{N}_{\mathrm{null}})} \quad Q^m_{(\mathcal{N}_{\mathrm{Qm}})} \quad Q^m_{(\mathcal{N}_{\mathrm{null}})}\right]. \tag{7}$$

Finally, the set of equations $h(x)$ is:

$$\begin{aligned} U_i^m &= U_i + \varepsilon_{U_i} \\ P_i^m &= h_{P_i}(U,\theta) + \varepsilon_{P_i} \\ Q_i^m &= h_{Q_i}(U,\theta) + \varepsilon_{Q_i} \end{aligned} \tag{8}$$

where the functions $h_{P_i}(U,\theta)$ and $h_{Q_i}(U,\theta)$ are:

$$\begin{aligned} h_{P_i}(U,\theta) &= U_i \cdot \sum_{k=1}^{n} U_k\left(G_{i,k}\cdot\cos(\theta_i-\theta_k) + B_{i,k}\cdot sen(\theta_i-\theta_k)\right) \\ h_{Q_i}(U,\theta) &= U_i \cdot \sum_{k=1}^{n} U_k\left(-B_{i,k}\cdot\cos(\theta_i-\theta_k) + G_{i,k}\cdot sen(\theta_i-\theta_k)\right) \end{aligned} \tag{9}$$

Thus, the following matrix H results:

$$H = \left[\begin{array}{c|c} \dfrac{\partial U^m}{\partial\theta} & \dfrac{\partial U^m}{\partial U} \\ \hline \dfrac{\partial h_P}{\partial\theta} & \dfrac{\partial h_P}{\partial U} \\ \hline \dfrac{\partial h_Q}{\partial\theta} & \dfrac{\partial h_Q}{\partial U} \end{array}\right]_{x^{(k}} \begin{array}{l} \left\{U_i^m = U_i + \varepsilon_{U_i}\right. \\ \left.i \in \mathcal{N}_{Um}\right. \\ \left\{P_i^m = h_{P_i}(U,\theta) + \varepsilon_{P_i}\right. \\ \left.i \in \mathcal{N}_{Pm} \cup \mathcal{N}_{null}\right. \\ \left\{Q_i^m = h_{Q_i}(U,\theta) + \varepsilon_{Q_i}\right. \\ \left.i \in \mathcal{N}_{Qm} \cup \mathcal{N}_{null}\right. \end{array} = \left[\begin{array}{c|c} 0 & 1_{(\mathcal{N}_{Um},\mathcal{N}} \\ \hline \dfrac{\partial h_P}{\partial\theta} & \dfrac{\partial h_P}{\partial U} \\ \hline \dfrac{\partial h_Q}{\partial\theta} & \dfrac{\partial h_Q}{\partial U} \end{array}\right]_{x^{(k}} \tag{10}$$

$$\overbrace{\theta_i\,,\, i\in\mathcal{N}\text{-}n_R} \qquad \overbrace{U_i\,,\, i\in\mathcal{N}}$$

In the previous equation, it must be considered that the matrix $1_{(NUm,N)}$ is a matrix with the size $N_{\mathrm{Um}} \times N$ with its elements at one when the corresponding measurement variable can be directly related to a state variable. For example, when the complete nodes vector is N={1,2,3,4,5}, and the node vector with voltage measurements is N_{Um} = {1,2,5}, the array $\partial U^m/\partial U$ can be represented as follows:

$$\frac{\partial U^m_{\{1,2,5\}}}{\partial U_{\{1,2,3,4,5\}}} = \begin{bmatrix} 1 & 0 & 0 & 0 & 0 \\ 0 & 1 & 0 & 0 & 0 \\ 0 & 0 & 0 & 0 & 1 \end{bmatrix} = 1_{(\{1,2,5\},\{1,2,3,4,5\}} \tag{11}$$

When a state estimator is used, a typical concern is the observability of the system, which implies considerations regarding topology and measurements. A network is observable if it has at least $2n-1$ measurements with $n-1$ measurements of P and n measurements of U or Q due to decoupling between P–U and between Q-δ. Furthermore, the rank of the matrix H must be equal to the number of variables for the state vector x. Therefore, a wind farm is observable with the typical measurements U, P and Q on the low voltage side of the WTGs and the high voltage side of the substation. However, it has little redundancy because the lack of only two measured values for P or Q renders the system unobservable. As shown in the following paragraphs, one objective of the proposed SE method is to increase the observability robustness.

2.2. Constrained state estimator

For nodes with virtual or exact measurements, it is necessary to consider the optimization problem as a constrained problem [11].

$$\begin{aligned} \text{Measurements}: \quad & z = h(x) + \varepsilon \\ \text{Virtual measurements}: \quad & c(x) = 0 \end{aligned} \tag{12}$$

For example, wind farms have interconnection nodes, where the injected active and reactive powers equal zero (see the nodes from 31 to 55 in Fig. 13). The constrained SE problem can be presented as an optimization problem and expressed as follows:

$$\begin{aligned} \min\{J(x)\} &= \min\left\{[z-h(x)]^T \cdot W \cdot [z-h(x)]\right\} \\ \text{restricted to}: \quad & c(x) = 0 \end{aligned} \tag{13}$$

From LaGrange theory, optimization with constraints of the functional J can be rewritten as a new functional to minimize J':

$$\min\{J'(x)\} = \min\left\{\frac{1}{2}\cdot[z^m - h(x)]^T \cdot W \cdot [z^m - h(x)] - \lambda^T \cdot [d - c(x)]\right\}. \tag{14}$$

Considering that $x^{(k+1)} = x^{(k)} + \Delta x^{(k)}$, this equation can be solved iteratively [11] [12]:

$$\begin{bmatrix} H^T \cdot W \cdot H & C^T \\ C & 0 \end{bmatrix} \cdot \begin{bmatrix} \Delta x^{(k)} \\ \lambda^{(k)} \end{bmatrix} = \begin{bmatrix} H^T \cdot W \cdot \left(z^m - h\left(x^{(k)}\right)\right) \\ -c\left(x^{(k)}\right) \end{bmatrix} \tag{15}$$

where the array H is:

$$H = \begin{bmatrix} 0 & I_{(\mathcal{N}_{Um}-\mathcal{N})} \\ \frac{\partial h_P}{\partial \theta} & \frac{\partial h_P}{\partial U} \\ \frac{\partial h_Q}{\partial \theta} & \frac{\partial h_Q}{\partial U} \end{bmatrix} \begin{cases} U_i^m = U_i + \varepsilon_{U_i} \\ i \in \mathcal{N}_{Um} \\ P_i^m = h_{P_i}(U,\theta) + \varepsilon_{P_i} \\ i \in \mathcal{N}_{Pm} \\ Q_i^m = h_{Q_i}(U,\theta) + \varepsilon_{Q_i} \\ i \in \mathcal{N}_{Qm} \end{cases}$$

$$\overbrace{\theta_i,\ i \in \mathcal{N}\text{-}n_R} \qquad \overbrace{U_i,\ i \in \mathcal{N}} \tag{16}$$

The constraints matrix *C*, where the injected active and reactive powers equal to zero, is:

$$C = \begin{bmatrix} \frac{\partial h_P}{\partial \theta} & \frac{\partial h_P}{\partial U} \\ \frac{\partial h_Q}{\partial \theta} & \frac{\partial h_Q}{\partial U} \end{bmatrix} \begin{cases} P_i = 0 = h_{P_i}(U,\theta) \\ i \in \mathcal{N}_{Pnull} \\ Q_i = 0 = h_{Q_i}(U,\theta) \\ i \in \mathcal{N}_{Qnull} \end{cases} \tag{17}$$

$$\overbrace{\theta_i,\ i \in \mathcal{N}\text{-}n_R} \qquad \overbrace{U_i,\ i \in \mathcal{N}}$$

3. Extended state estimator

In this section, the proposed SE method (extended state estimator) is presented, wherein equations relating the WTG variables active power, reactive power, voltage and reactive power generated at the capacitor banks are incorporated into the state estimator. Therefore, the state variable vector was extended to include the new variables. Similarly, any voltage measurements with the corresponding state variable, active and reactive power injected at the WTG nodes, will be included in the extended state vector:

$$x_e = \left[\, \theta_{(\mathcal{N}-n_R)} \quad U_{(\mathcal{N})} \quad P_{(\mathcal{N}_e)} \quad Q_{(\mathcal{N}_e)} \,\right] \tag{18}$$

Including the new variables implies that the equations for P_i^m and Q_i^m at the WTG nodes (see (9)) are rewritten to consider the new state variables:

$$\begin{aligned} P_i^m = h_{P_i}(U,\theta) + \varepsilon_{P_i} &\Leftrightarrow \begin{cases} \mathrm{P_i^m} = \mathrm{P_i} + \varepsilon_{\mathrm{P_i}} \\ \mathrm{h_{P_i}(U,\theta) - P_i} = 0 \end{cases} \\ Q_i^m = h_{Q_i}(U,\theta) + \varepsilon_{Q_i} &\Leftrightarrow \begin{cases} \mathrm{Q_i^m} = \mathrm{Q_i} + \varepsilon_{\mathrm{Q_i}} \\ \mathrm{h_{Q_i}(U,\theta) - Q_i} = 0 \end{cases} \end{aligned} \tag{19}$$

Due to these modifications, the equations that relate voltage as well as active and reactive power in the WTGs can be included:

$$h_e\left(U_{(\mathcal{N}_e)}, P_{(\mathcal{N}_e)}, Q_{(\mathcal{N}_e)}\right) = 0 \tag{20}$$

These equations are included in the proposed SE as constraints. They were obtained as depicted in the following section.

Based on the previous definitions, an extended Jacobian matrix H_e, was defined as follows and considers the new set of variables:

$$H_e = \begin{bmatrix} 0 & I_{(\mathcal{N}_{Um}-\mathcal{N})} & 0 & 0 \\ 0 & 0 & I_{(\mathcal{N}_{Pm}-\mathcal{N}_e)} & 0 \\ 0 & 0 & 0 & I_{(\mathcal{N}_{Qm}-\mathcal{N}_e)} \\ \frac{\partial h_P}{\partial \theta} & \frac{\partial h_P}{\partial U} & 0 & 0 \\ \frac{\partial h_Q}{\partial \theta} & \frac{\partial h_Q}{\partial U} & 0 & 0 \end{bmatrix} \begin{cases} U_i^m = U_i + \varepsilon_{U_i} \\ i \in \mathcal{N}_{Um} \\ P_i^m = P_i + \varepsilon_{P_i} \\ i \in \mathcal{N}_{Pm} \cap \mathcal{N}_e \\ Q_i^m = Q_i + \varepsilon_{Q_i} \\ i \in \mathcal{N}_{Qm} \cap \mathcal{N}_e \\ P_i^m = h_{P_i}(U,\theta) + \varepsilon_{P_i} \\ i \in \mathcal{N}_{Pm}\text{-}\mathcal{N}_e \\ Q_i^m = h_{Q_i}(U,\theta) + \varepsilon_{Q_i} \\ i \in \mathcal{N}_{Qm}\text{-}\mathcal{N}_e \end{cases} \tag{21}$$

$$\overbrace{\theta_i,i\in\mathcal{N}-n_R} \quad \overbrace{U_i,i\in\mathcal{N}} \quad \overbrace{P_i,i\in\mathcal{N}_e} \quad \overbrace{Q_i,i\in\mathcal{N}_e}$$

In addition, the extended constrained matrix C_e is:

$$C_e = \begin{bmatrix} \frac{\partial h_P}{\partial \theta} & \frac{\partial h_P}{\partial U} & 0 & 0 \\ \frac{\partial h_Q}{\partial \theta} & \frac{\partial h_Q}{\partial U} & 0 & 0 \\ \frac{\partial h_P}{\partial \theta} & \frac{\partial h_P}{\partial U} & -I_{(\mathcal{N}_{Pm}-\mathcal{N}_e)} & 0 \\ \frac{\partial h_Q}{\partial \theta} & \frac{\partial h_Q}{\partial U} & 0 & -I_{(\mathcal{N}_{Qm}-\mathcal{N}_e)} \\ 0 & \frac{\partial h_e}{\partial U} & \frac{\partial h_e}{\partial P} & \frac{\partial h_e}{\partial Q} \end{bmatrix} \begin{cases} P_i^m = h_{P_i}(U,\theta) = 0 \\ i \in \mathcal{N}_{Pnull} \\ Q_i^m = h_{Q_i}(U,\theta) = 0 \\ i \in \mathcal{N}_{Qnull} \\ h_{P_i}(U,\theta) - P_i = 0 \\ i \in \mathcal{N}_{Pm} \cap \mathcal{N}_e \\ h_{Q_i}(U,\theta) - Q_i = 0 \\ i \in \mathcal{N}_{Qm} \cap \mathcal{N}_e \\ h_{e_i}(U_i,P_i,Q_i) = 0 \\ i \in \mathcal{N}_e \end{cases} \tag{22}$$

$$\overbrace{\theta_i,i\in\mathcal{N}-n_R} \quad \overbrace{U_i,i\in\mathcal{N}} \quad \overbrace{P_i,i\in\mathcal{N}_e} \quad \overbrace{Q_i,i\in\mathcal{N}_e}$$

The resulting system of equations can be solved using (15). Furthermore, it must be considered that when the measurements in any WTG are unavailable, only their corresponding equations are excluded from the extended matrix H_e.

The proposed methodology for the extended SE is shown in Fig. 2, where the relationship between the WTG models, measurement data and estimator is depicted, which can be compared with the classical SE shown in Fig. 1. The main characteristics of the proposed method are the following:

- Including the WTG models is the SE with constrains
- Extended state vector includes all variables measured for the WTGs.
- WTG modeling from measurement data using BPNNs and polynomial fitting.

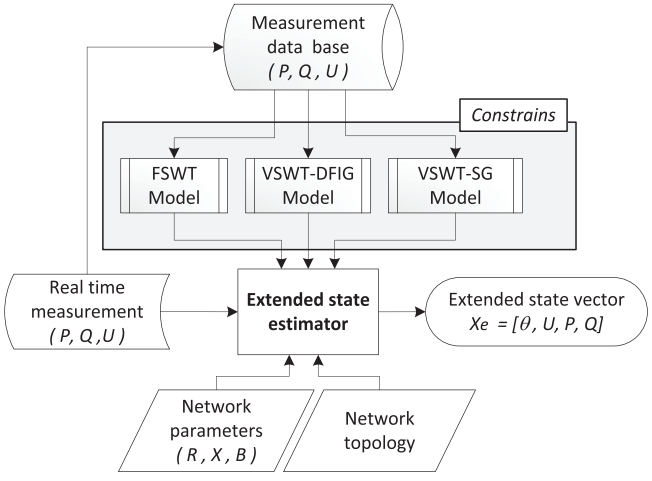

Fig. 2. Implementation methodology for the proposed extended state estimator.

Table 1
Wind turbines installed in the Sotavento wind park.

Wind turbine model	Number label	Power (kW)	Generator	Pitch/Speed
Izar-Bonus 1.3 Mw	1	1300	IG	Variable/Variable
Made AE − 46	6, 10, 17, 23	660	IG	Fixed/Fixed
Neg Micon NM-750	2, 8, 13, 20	750	IG	Fixed/Fixed
Neg Micon NM-900	12	900	IG	Fixed/Fixed
Ecotecnia 44 − 640	4, 11, 15, 21	640	IG	Fixed/Fixed
Made AE-52	16	800	SG	Variable/Variable
Izar-Bonus MK − IV	5, 9, 18, 22	600	IG	Fixed/Fixed
Gamesa G-47	3, 7, 14, 19	660	DFIG	Variable/Variable
Made AE − 61	24	1320	IG	Fixed/Fixed

Table 2 shows a summary of the types of WTGs, the equations used to model them, the modeling technique and the variables as well as parameters involved. The modeling results have been evaluated using the typical fitness indicators: the coefficient of determination (R2) and the root-mean-square error (RMSE).

4. WTG modeling

The WTG equations are included in the proposed extended SE using [20]. These equations model the WTG behavior by relating voltage, active power and reactive power. Based on the WTGs installed in the Sotavento wind park [15], the following three WTG technologies were considered in this paper:

- Fixed speed WTG based on an induction generator (FSWT)
- Variable speed WTG based on a doubly fed induction generator (VSWT-DFIG)
- Variable speed WTG based on a synchronous generator with an AC/AC back-to-back converter (VSWT-SG)

The following paragraphs describe the method for obtaining the functions that model behavior for the different types of WTGs. In this paper, to generate these models, measurement data were used from studying the wind park SCADA for one year. All WTGs were modeled using BPNNs trained from measurement data or by fitting polynomials. In the following paragraphs, the equations related to each technology are depicted, and the results of the BPNN modeling are shown.

4.1. Fixed speed WTG based on induction generator (FSWT)

To model an FSWT, three variables must be included in the extended state vector: the active power P_i and reactive power Q_i injected by the WTG, as well as the reactive power Q_{Ci} generated at the capacitor bank. This construction implies that the following equations are used:

$$\left.\begin{array}{l} P_i^m = P_i + \varepsilon_{Pi} \\ Q_i^m = Q_i + \varepsilon_{Qi} \\ Qc_i^m = Qc_i + \varepsilon_{Q_i} \\ h_{P_i}(U,\theta) - P_i = 0 \\ h_{Q_i}(U,\theta) - Q_i = 0 \\ h_{e,IG_i}(U_i, P_i, Q_i, Q_{Ci}) = 0 \end{array}\right\} i \in N_{e,IG} \tag{23}$$

where $h_{e,\mathrm{FSWTi}}$ is the function that models the ith FSWT. This function was obtained using BPNNs, as shown below.

An FSWT is formed by an induction generator and a power factor controller (PFC), which controls the different capacitor bank

Table 2
Modeling parameters and test results for all WTs.

Type	Function	Modeling	Model parameters	WT	Test	
					R2	RMSE
FSWT	$h_{e,IG_i}(U_i, P_i, Q_i, Q_{Ci}) = 0$	BPNN	Input vector: [*P*, *Q*, *U*]	1	0.992	0.0054
			Target vector: [Q_c]	2	0.928	0.0031
			Layers: [3 5 30 1]	4	0.989	0.0014
			Transfer functions: *tansig*, *tansig*, *purelin*	5	0.980	0.0031
			Training method: Levenberg–Marquardt	6	0.997	0.0020
			Perf. goal: 10^{-6}	8	0.917	0.0026
			Min. perf. gradient: 10^{-6}	9	0.942	0.0025
				10	0.997	0.0022
				11	0.992	0.0016
				12	0.940	0.0014
				13	0.981	0.0025
				15	0.992	0.0014
				17	0.997	0.0019
				18	0.962	0.0017
				20	0.904	0.0033
				21	0.993	0.0014
				22	0.967	0.0025
				23	0.988	0.0024
				24	0.967	0.0028
VSWT-DFIG	$h_{e,DFIG_{I,i,j}}(P_{Rj}, P_{Si}) = 0$	BPNN	Input vector: [P_S]	3	0.983	2.4844
			Target vector: [P_R]	7	0.973	2.8881
			Layers: [1 5 10 1]	14	0.966	2.9718
			(similar to the previous BPNNs)	19	0.959	3.1924
	$h_{e,DFIG_{II,j}}(P_{Rj}, Q_{Rj}) = 0$	Fitted function	Input vector: [P_R]	3	0.992	0.6833
			Output vector: [Q_R]	7	0.994	0.6850
				14	0.996	0.6433
				19	0.998	0.6057
	$h_{e,DFIG_{III,i}}(P_{Si}, Q_{Si}) = 0$	Fitted function	Input vector: [P_S]	3	0.990	0.2491
			Output vector: [Q_S]	7	0.992	0.2395
				14	0.992	0.2369
				19	0.993	0.2110
VSWT-SG	$h_{e,SG_i}(U_i, P_i, Q_i) = 0$	Fitted function	Input vector: [*P*, *U*]	16	0.973	1.7017
			Output vector: [*Q*]			

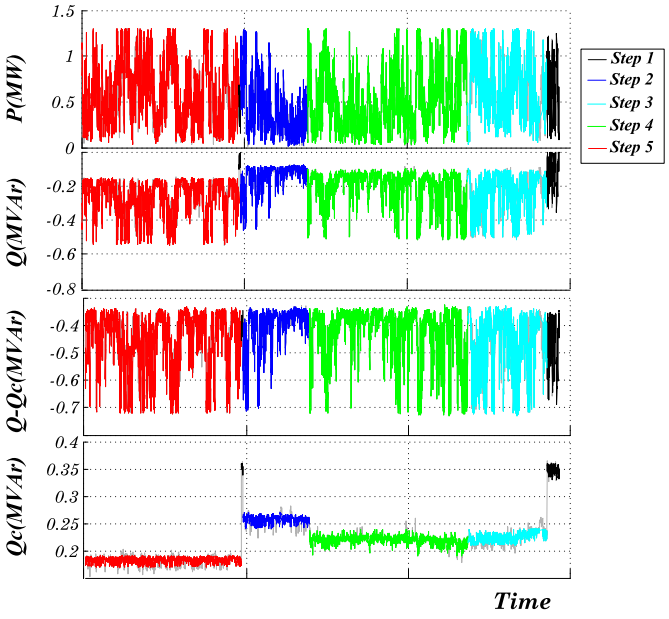

Fig. 3. Output Q_c against time estimated using a BPNN for an FSWT Izar-Bonus 1.3 MW.

steps. Therefore, to model this WTG, the models and their corresponding parameters for the generator and PFC are necessary. That type of information is not typically provided by the WTG manufacturer. Furthermore, the PFC model may require representation by a logical function that cannot be included in the SE due to its inherent discontinuities. To overcome these inconveniences, a BPNN is proposed to obtain $h_{e,\mathrm{FSWTi}}$ (see Appendix IX.B); thus, the resulting function is differentiable and can be included in the SE (see Appendix IX.A). The BPNN output is shown in Figs. 3 and 4.

The reactive power generated by the shunt capacitors (Q_{Ci}) can be included in the extended SE in several ways, depending on the available measurements:

- When Q_{Ci} measurements are available (Q^m_{Ci}; see Fig. 5), it is sufficient to consider the equation that relates Q^m_{Ci} with the variable Q_{Ci} in matrix H as follows:

$$Q^m_{\mathrm{Ci}} = Q_{\mathrm{Ci}} + \varepsilon. \tag{24}$$

- When the status of the PFC is available (see Fig. 6), a similar procedure to the previous case can be used [16]. The measurement values Q^m_{Ci} can be obtained using the following:

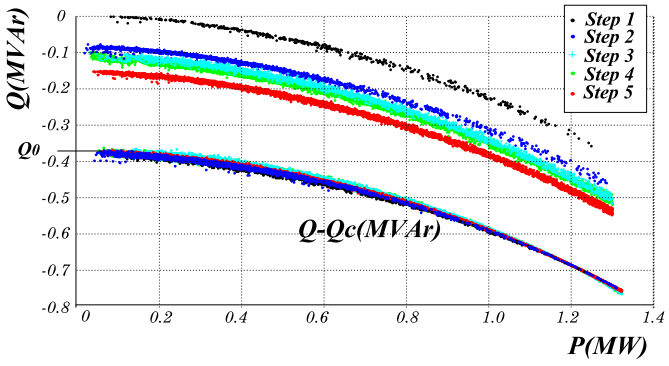

Fig. 4. P-Q diagram for an FSWT Izar-Bonus 1.3 MW.

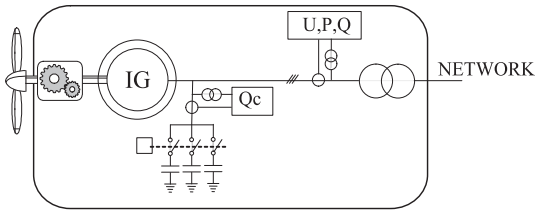

Fig. 5. Induction generator with measurements for U_i, P_i, Q_{Gi} and Q_{Ci}.

$$Q^m_{\mathrm{Ci}} = \left(\frac{U_i}{U_N}\right)^2 \cdot \sum_{j=1}^{N_{\mathrm{Ci}}} Q_{C_{ij}} b_{ij} \tag{25}$$

where N_{Ci} is the number of capacitor steps in the ith FSWT, b_{ij} is a binary variable that indicates the status of the jth step, U_n is the capacitor-rated voltage, and Q_{Cij} is the rated reactive power for each capacitor step.

4.2. Variable-speed WTG based on a doubly fed induction generator (VSWT-DFIG)

To model VSWT-DFIG machines, four variables must be included in the extended SE (see Fig. 7): the active and reactive power on the rotor side (P_{Ri}, Q_{Ri}), as well as the active and reactive power on the stator side (P_{Si}, Q_{Si}). The following equations relate the active and reactive power injection on the rotor and stator sides and must be considered:

$$\left.\begin{aligned} P^m_{Rj} &= P_{Rj} + \varepsilon_{PRj} \\ P^m_{Si} &= P_{Si} + \varepsilon_{PSi} \\ Q^m_{Rj} &= Q_{Rj} + \varepsilon_{PRj} \\ Q^m_{Si} &= Q_{Si} + \varepsilon_{PSi} \\ h_{Pi}(U,\theta) - P_{Si} &= 0 \\ h_{Pj}(U,\theta) - P_{Rj} &= 0 \\ h_{Qi}(U,\theta) - Q_{Si} &= 0 \\ h_{Qj}(U,\theta) - Q_{Rj} &= 0 \end{aligned}\right\} \begin{matrix} i \in N_{e,DFIGS} \\ j \in N_{e,DFIGR} \end{matrix} \tag{26}$$

$$h_{e,DFIG_{I,i,j}}(P_{Rj}, P_{Si}) = 0 \Big\} \begin{matrix} i \in N_{e,DFIGS} \\ j \in N_{e,DFIGR} \end{matrix} \tag{27}$$

$$h_{e,DFIG_{II,j}}(P_{Rj}, Q_{Rj}) = 0 \Big\} j \in N_{e,DFIGR} \tag{28}$$

$$h_{e,DFIG_{III,i}}(P_{Si}, Q_{Si}) = 0 \Big\} i \in N_{e,DFIGS} \tag{29}$$

where (27), (28) and (29) are the equations that model the ith VSWT-DFIG. It must be considered that in these types of WTGs, two sets of nodes must be considered: one set includes the nodes on the stator side, and the other set includes the nodes on the rotor side. Finally, the relationship in (27) was obtained using BPNNs with measured powers from the stator and rotor sides for a Gamesa G47 VSWT-DFIG. The behavior of the resulting function is shown in Fig. 8.

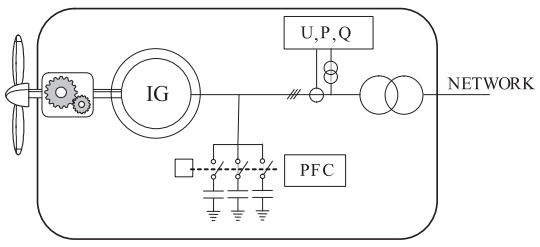

Fig. 6. Induction generator with measurements for the U_i, P_i, Q_i and PFC status.

Due to their simplicity, the remaining equations (28) and (29) were obtained using a polynomial obtained by fitting techniques and measured data.

Using the above-described fitting technique, the resulting relationship for equation (28) is:

$$h_{e,\mathrm{DFIG}_{II,i}}(P_{\mathrm{Si}}, Q_{\mathrm{Si}}) = Q_{Si} - a\cdot P_{\mathrm{Si}}^2 + b\cdot P_{\mathrm{Si}} + c = 0 \tag{30}$$

where the coefficients a, b and c are defined using the power factor setpoint (PFp) as a parameter.

$$\begin{aligned} a &= -3.8571\cdot PFp + 3.905 \\ b &= \pm\tan\left(\mathrm{acos}\left(PFp\right)\right) \quad \text{where} \begin{cases} - & \text{if } PFp \text{ inductive} \\ + & \text{if } PFp \text{ capacitive} \end{cases} \\ c &= 0 \end{aligned} \tag{31}$$

For example, Fig. 9 shows the measured values compared with the values obtained using a fitted function for different power factor setpoint values. Similarly, equation (29) can be defined using the following linear equation:

$$\begin{aligned} &h_{e,DFIG_{III},j}(P_{Rj}, Q_{Rj}) = Q_{Rj} - a\cdot P_{Rj} + b = 0 \\ &a = 0.109 \\ &b = 0.002337 \end{aligned} \tag{32}$$

Fig. 10 shows the measured values compared with the values obtained using the fitted function.

4.3. Variable-speed WTG based on a synchronous generator with an AC/AC converter (VSWT-SG)

To include VSWT-SGs in the extended SE, two variables must be considered: the active power P_i and reactive Q_i injected at the WTG node; this construction implies that the equation relating the active power to the reactive power must be considered, which yields the following:

$$\begin{aligned} &P_i^m = P_i + \varepsilon_{Pi} \\ &Q_i^m = Q_i + \varepsilon_{Qi} \\ &h_{P_i}(U,\theta) - P_i = 0 \\ &h_{Q_i}(U,\theta) - Q_i = 0 \end{aligned} \Big\} i \in N_{e,SG} \tag{33}$$

$$h_{e,SG_i}(U_i, P_i, Q_i) = 0 \;\} i \in N_{e,SG} \tag{34}$$

where equation (34) models the ith VSWT-SG. This type of WTG has an AC/AC back-to-back converter between the generator and low voltage side of the transformer (see Fig. 11). Theoretically, this construction yields the capability to control the WTG and maintain a constant power factor setpoint; however, this is not always generated in real machines. As in the previous section, this equation can be obtained by fitting measurement data with a linear function, wherein the parameters depend on the power factor setpoint. For example, the resulting values obtained with the fitted function are compared with measurements in Fig. 12.

4.4. The extended state estimator

Using the FSWT, VSWT-DFIG and VSWT-SG relationships, the proposed extended Jacobian matrix H_e and matrix of constraints C_e were generated and can be written as:

$$H = \begin{bmatrix} 0 & I_{(N_{Um},N)} & 0 & 0 & 0 \\ 0 & 0 & I_{(N_{Pm},N_e)} & 0 & 0 \\ 0 & 0 & 0 & I_{(N_{Qm},N_e)} & 0 \\ 0 & 0 & 0 & 0 & I_{(N_{Qcm},N_e)} \\ \frac{\partial h_P}{\partial\theta} & \frac{\partial h_P}{\partial U} & 0 & 0 & 0 \\ \frac{\partial h_Q}{\partial\theta} & \frac{\partial h_Q}{\partial U} & 0 & 0 & 0 \end{bmatrix} \begin{matrix} \{U_i^m = U_i + \varepsilon_{U_i},\ i\in N_{Um} \\ \{P_i^m = P_i + \varepsilon_{P_i},\ i\in N_{Pm}\cap N_e \\ \{Q_i^m = Q_i + \varepsilon_{Q_i},\ i\in N_{Qm}\cap N_e \\ \{Qc_i^m = Qc_i + \varepsilon_{Qc_i},\ i\in N_{Qcm}\cap N_e \\ \{P_i^m = h_{P_i}(U,\theta) + \varepsilon_{P_i},\ i\in N_{Pm}-N_e \\ \{Q_i^m = h_{Q_i}(U,\theta) + \varepsilon_{Q_i},\ i\in N_{Qm}-N_e \end{matrix} \tag{35}$$

$$\underbrace{\theta_i, i\in N-n_R}\quad \underbrace{U_i, i\in N}\quad \underbrace{P_i, i\in N_e}\quad \underbrace{Q_i, i\in N_e}\quad \underbrace{Qc_i, i\in N_{e,FSWT}}$$

$$C = \begin{bmatrix} \frac{\partial h_P}{\partial\theta} & \frac{\partial h_P}{\partial U} & -1 & 0 & \\ \frac{\partial h_Q}{\partial\theta} & \frac{\partial h_Q}{\partial U} & 0 & -1 & \\ \frac{\partial h_P}{\partial\theta} & \frac{\partial h_P}{\partial U} & 0 & 0 & \\ \frac{\partial h_Q}{\partial\theta} & \frac{\partial h_Q}{\partial U} & 0 & 0 & \\ 0 & \frac{\partial h_{e,FSWT}}{\partial U} & \frac{\partial h_{e,FSWT}}{\partial P} & \frac{\partial h_{e,FSWT}}{\partial Q} & \frac{\partial h_{e,FSWT}}{\partial Q_C} \\ & & \frac{\partial h_{e,VSWT-DFIG,I}}{\partial P} & & \\ & & \frac{\partial h_{e,VSWT-DFIG,II}}{\partial P} & \frac{\partial h_{e,VSWT-DFIG,II}}{\partial Q} & \\ & & \frac{\partial h_{e,VSWT-DFIG,III}}{\partial P} & \frac{\partial h_{e,VSWT-DFIG,III}}{\partial P} & \\ & \frac{\partial h_{e_{SG}}}{\partial U} & \frac{\partial h_{e_{SG}}}{\partial P} & \frac{\partial h_{e_{SG}}}{\partial Q} & \end{bmatrix} \begin{matrix} \{h_{P_i}(U,\theta) - P_i = 0 \\ \{h_{Q_i}(U,\theta) - Q_i = 0 \\ \\ \{P_i^m = h_{P_i}(U,\theta) = 0 \\ \{Q_i^m = h_{Q_i}(U,\theta) = 0 \\ \\ FSWT \\ \{h_{e,FSWT}(U,P,Q,Q_C) = 0 \\ \\ VSWT-DFIG \\ \{h_{e,VSWT-DFIG,I}(P) = 0 \\ \{h_{e,VSWT-DFIG,II}(P,Q) = 0 \\ \{h_{e,VSWT-DFIG,III}(P,Q) = 0 \\ \\ VSWT-SG \\ \{h_{e,VSWT-SG}(U,P,Q) = 0 \end{matrix} \tag{36}$$

$$\underbrace{\theta_i}_{i\in N-n_R}\quad \underbrace{U_i}_{i\in N}\quad \underbrace{P_i}_{i\in N_e}\quad \underbrace{Q_i}_{i\in N_e}\quad \underbrace{Qc_i}_{i\in N_{e,FSWT}}$$

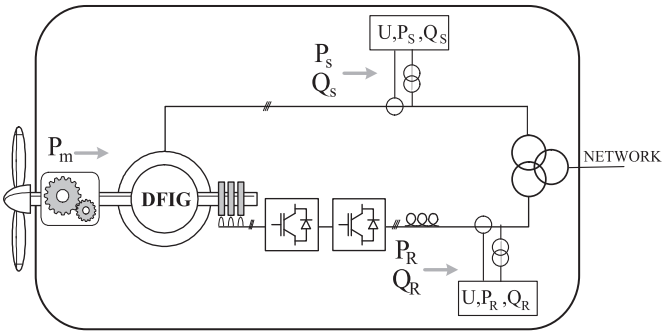

Fig. 7. VSWT-DFIG with measurements for U_i, P_i and Q_i on the rotor and stator sides.

5. Results for the Sotavento Experimental Wind Park

5.1. The wind park

The project is referred to as Sotavento Galicia S. A. It was created in 1997 and promoted by the Consellería de Industria e Comercio (Department for Industry and Trade), which is a department of Xunta de Galicia (local government). Its objective is to generate not only economic but also scientific and technical advantages. Three public institutions are involved in this project, which provided 51% of its capital. The Sotavento Experimental Wind Park (see Table 1 and Fig. 13) was formed by 24 WTGs with 17.56 MW total power and 38500 MWh/year estimated energy production.

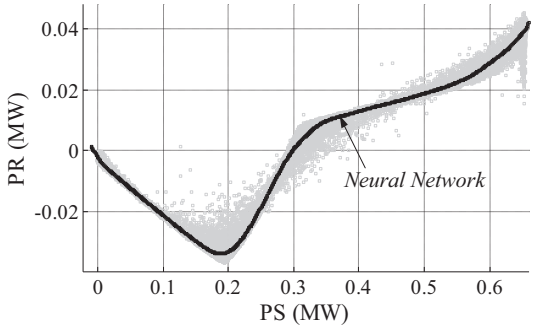

Fig. 8. Relationship between active power on the rotor and stator sides in a doubly-fed generator in a VSWT-DFIG Made AE46.

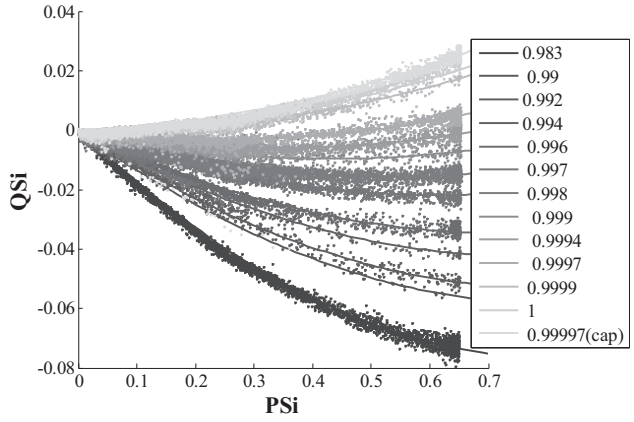

Fig. 9. Relationship between the active power P_{Si} and reactive power Q_{Si} on the stator side for different power factor setpoint values in the turbine Made AE46.

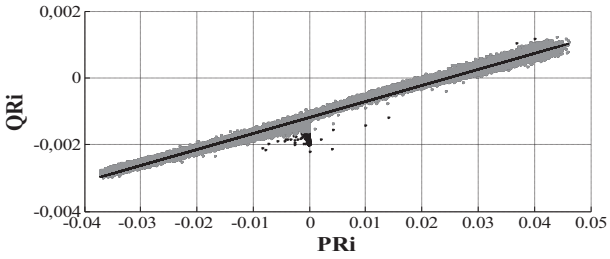

Fig. 10. Relationship between the active power P_{Ri} and reactive power Q_{Ri} on the rotor side for different power factor setpoint values in the turbine Made AE46.

5.2. Available measurements

Measurements are available at the Sotavento wind farm through the centralized monitoring system (SCADA), including real-time voltage, active power and reactive power on the low voltage side of the WTG transformers and the high voltage side of the substation. In addition, the P and Q measurements are available on the rotor and stator sides of the VSWT-DFIGs. Finally, the status of the PFCs for the WTGs and substation is known [16].

Considering the park configuration (see Fig. 13), the resulting network was formed by the following 60 nodes.

- 1–24: LV bars at 24 WTGs
- 25–28: rotor-side LV bars at the VSWT-DFIGs
- 29, 30: bars at the substation
- 31–54: MV bars at the 24 WTGs
- 55–56: LV and MV control building bars
- 57–60: virtual nodes used to model three winding transformers in VSWT-DFIGs.

The measurements for the nodes 31–55 and 57–60 are virtual ($P = 0$, $Q = 0$).

Therefore, the state vector is formed by 119 variables, and the extended vector of estate variables includes 188 elements. The total

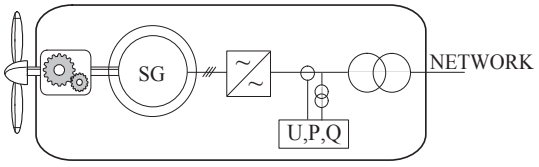

Fig. 11. Synchronous generator measurements for U_i, P_i and Q_i.

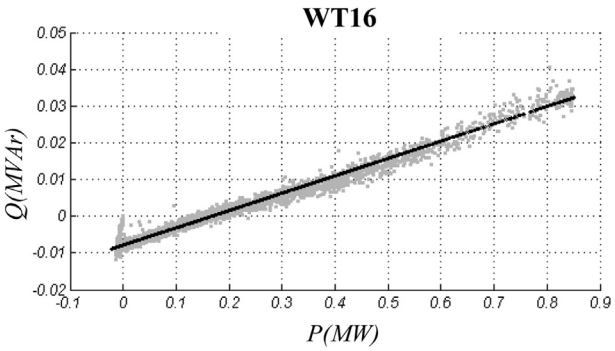

Fig. 12. Relationship between the active power P and reactive power Q injected at the WTG node in the turbine MADE AE52.

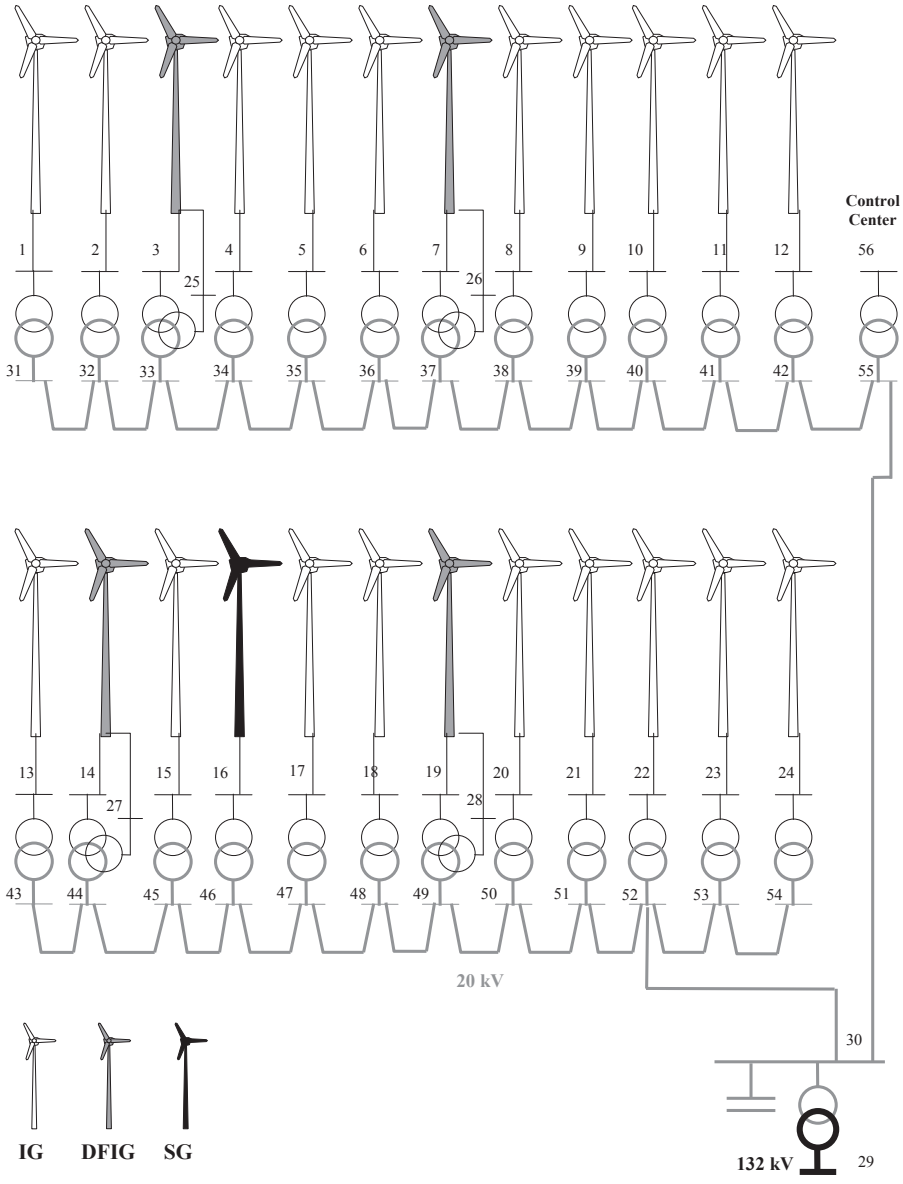

Fig. 13. Sotavento wind farm.

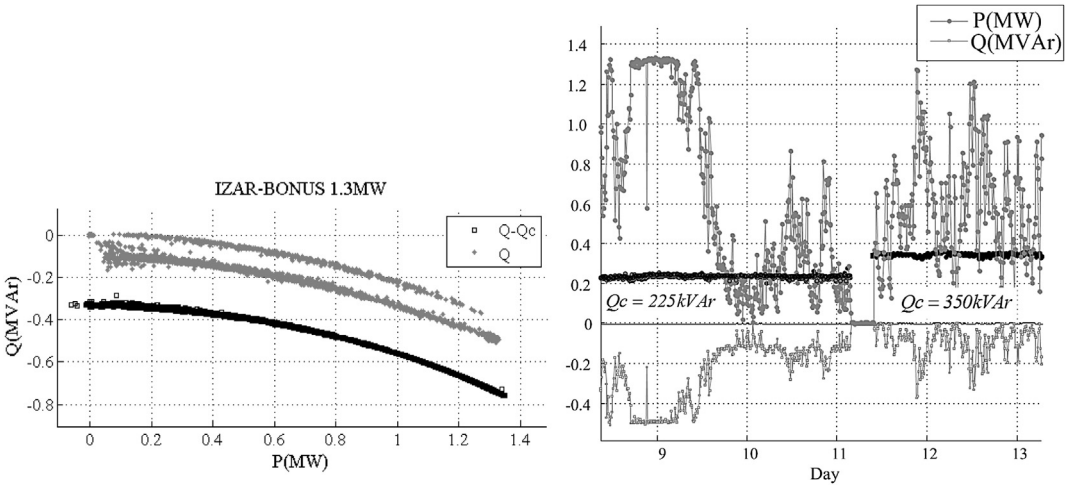

Fig. 14. P and Q for an FSWT Izar-Bonus 1.3 MW (the measurements are in gray, and the values obtained using SE are in black).

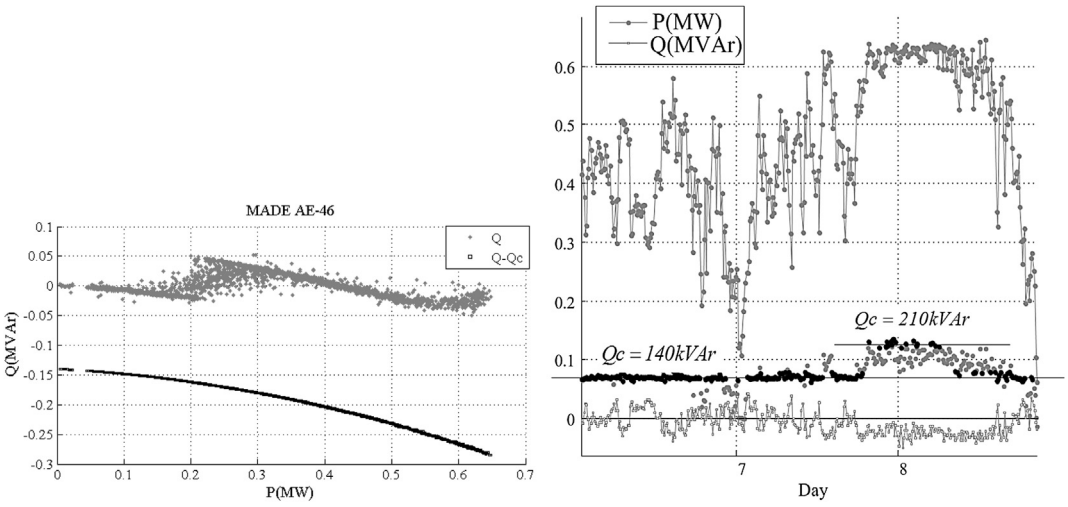

Fig. 15. P and Q for the FSWT Made AE-46 (the measurements are in gray, and the values obtained with SE are in black).

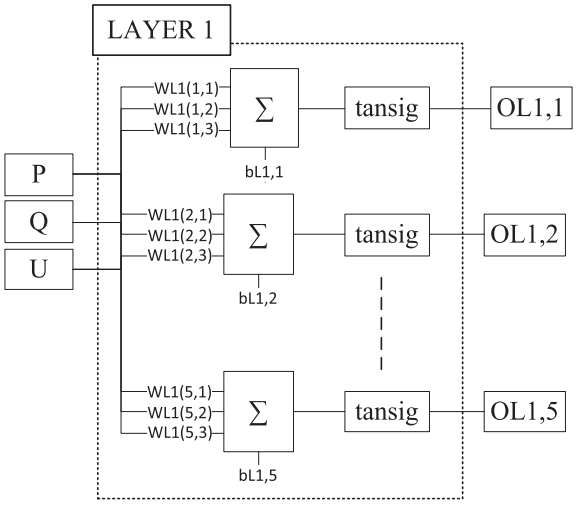

Fig. 16. Architecture for the input layer.

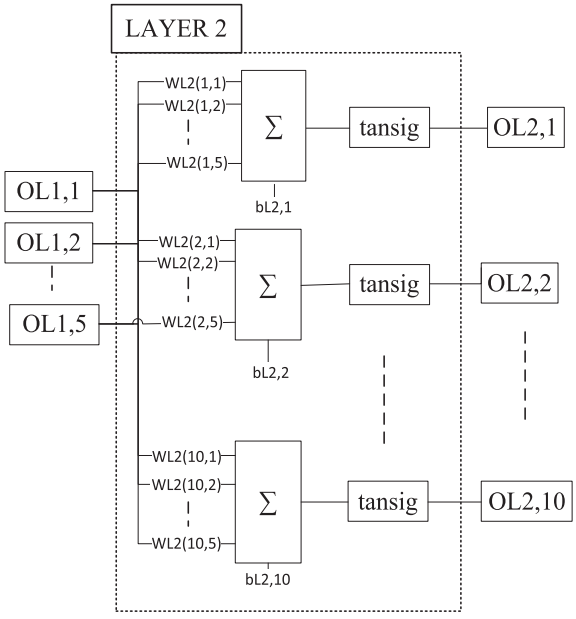

Fig. 17. Architecture for the hidden layer.

number of equations is 265; 109 are part of the extended Jacobian matrix H_e, and l56 are part of the extended matrix of constraint C_e.

5.3. Estimation results

To demonstrate operation of the proposed extended SE, the method was tested using measurement data recorded every 10 min over 30 days. Fig. 14 and Fig. 15 show the relationships between the active and reactive power for two FSWTs (Izar-Bonus 1.3 MW and Made AE-46) for which two different power factor correction systems were used.

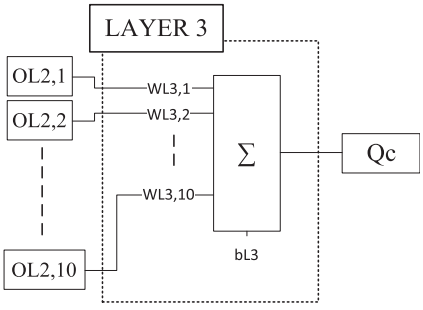

Fig. 18. Architecture for the output layer.

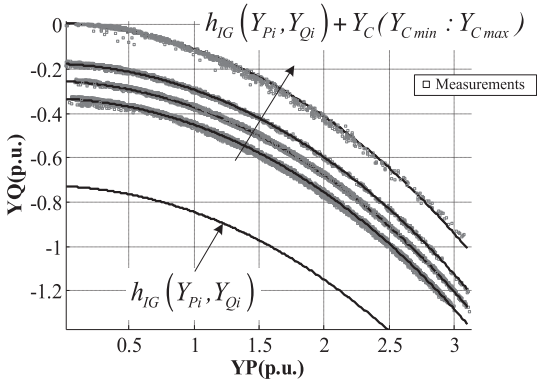

Fig. 19. Bonus 1.3 MW generator admittance.

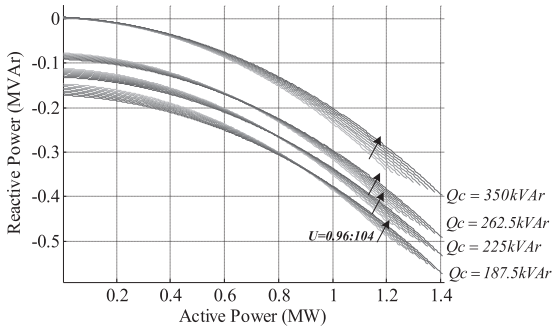

Fig. 20. Training pattern for the BPNN (Izar-Bonus 1.3 MW).

The modeling results were evaluated with the coefficient of determination (R2) and root-mean-square error (RMSE), as shown in Table 2.

Finally, Appendix IX.C presents the relationship between active and reactive power for each WTG at the wind park.

6. Conclusions

State estimation in wind parks is a useful tool for analyzing its operation conditions. Thus, the working state of the complete installation can be established, and another type of data can be derived, including out-of-service WTGs, aging capacitor banks, communication failures, energy loss estimates, and so on. However, the classic SE is not reliable for predicting behavior due to the typical decoupling between the active and reactive power in this

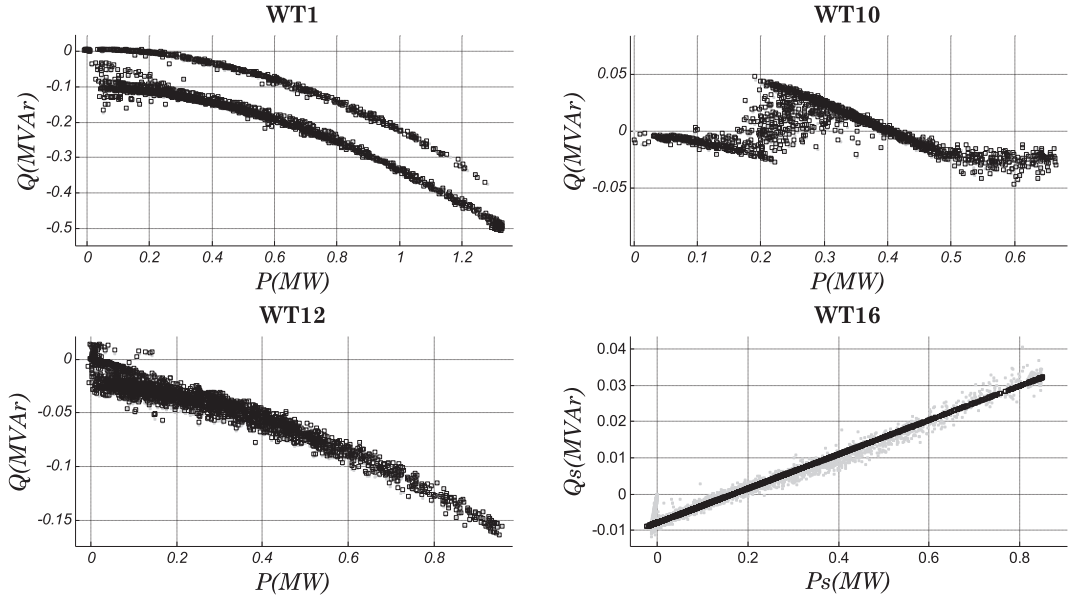

Fig. 21. Results for WT1, WT10, WT12 and WT16.

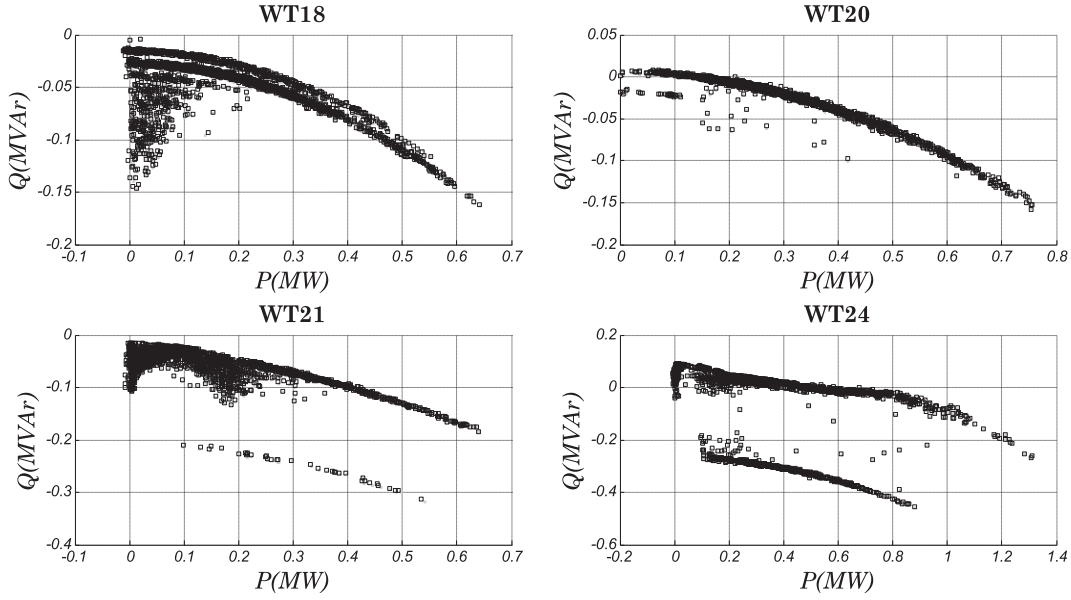

Fig. 22. Results for WT18, WT20, WT21 and WT24.

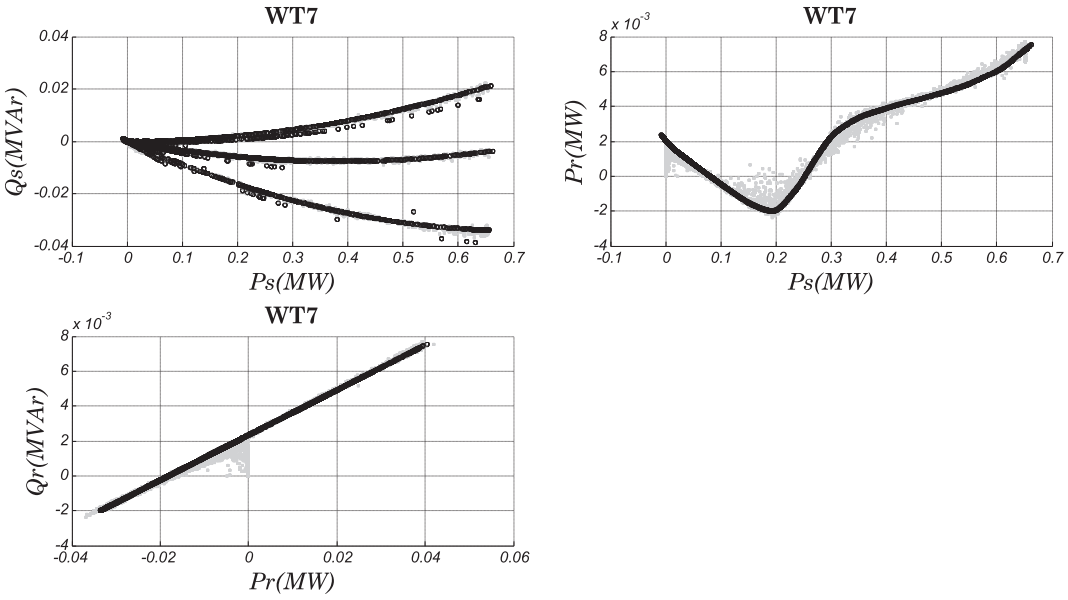

Fig. 23. Results for WT7.

type of installation. Thus, the solutions from classic SE may not be technically feasible (out-of-range values, unrealistic power flows and values that are incompatible with the WTG operation), and the system exhibits weak observability (the system is no longer observable when data from a single WTG is lost).

To overcome the aforementioned drawbacks, an extended SE is proposed herein, where the WTG models are incorporated into the equation system. To obtain a set of equations that can easily be included in the SE, polynomial fitting and BPNN techniques were used, which only require measurement data; thus, the WTG parameters are not necessary.

One consequence is that the decoupling between P–V and between Q-δ disappears; thus, solutions for the proposed method are always technically feasible, at least at the WTG level. Moreover, the method is more robust against a lack of measurements, which are typically due to communication errors or metering device failures.

The method has been tested using measurement data from Sotavento Wind Park, which includes WTGs for different types of technologies (FSWT, VSWT-DFIG and VSWT-SG).

Acknowledgments

The authors would like to thank the personnel of Sotavento Experimental Wind Park for their contribution and help with field experience as well as for their access to the measurement data.

This work was supported in part by the Consellería of Innovación e Industria (Xunta de Galicia, Spain), under the contract 07REM008V19PR, and the Ministry of Science and Innovation (Spain), under the contracts ENE 2007-67473 and ENE 2009-13074.

Appendix

A. Obtaining the derivative of a BPNN

Back propagation neural networks (BPNNs) [17] [18] are typically used as the best approximation for multivariable functions [19] that have no known analytical expression or are difficult to use. In this paper, a BPNN was used as an activation function based on a hyperbolic tangent [9]. As a consequence, the resulting neural networks are continuous and differentiable. Assuming that five neurons are in the input layer (see Fig. 16), the BPNN output can be written as follows:

$$\begin{bmatrix} \text{Out1} \\ \text{Out2} \\ \text{Out3} \\ \text{Out4} \\ \text{Out5} \end{bmatrix}_{L1} = \tan sig\left(\begin{bmatrix} W_{L1(1,1)} & W_{L1(1,2)} & W_{L1(1,3)} \\ W_{L1(2,1)} & W_{L1(2,2)} & W_{L1(2,3)} \\ W_{L1(3,1)} & W_{L1(3,2)} & W_{L1(3,3)} \\ W_{L1(4,1)} & W_{L1(4,2)} & W_{L1(4,3)} \\ W_{L1(5,1)} & W_{L1(5,2)} & W_{L1(5,3)} \end{bmatrix}_{L1} \times \begin{bmatrix} P \\ Q \\ U \end{bmatrix} + \begin{bmatrix} b_{L1,1} \\ b_{L1,2} \\ b_{L1,3} \\ b_{L1,4} \\ b_{L1,5} \end{bmatrix}_{L1} \right) \Rightarrow$$
$$[O_{L1}]_{5\times1} = \tan sig\left([W_{L1}]_{5\times3} \times [E_{L1}]_{3\times1} + [B_{L1}]_{5\times1}\right) \quad (37)$$

Next, the second hidden layer (assuming that it is formed by 10 neurons) with the same architecture as the input layer (see Fig. 17) is expressed as:

$$[O_{L2}]_{10\times1} = \tan sig\left([W_{L2}]_{10\times5} \times [O_{L1}]_{5\times1} + [B_{L2}]_{10\times1}\right) \quad (38)$$

Finally, the output layer (layer 3) (see Fig. 18) is a purelin-type layer, which yields the following equation:

$$Qc = [O_{L3}]_{1\times1} = \left([W_{L3}]_{1\times10} \times [O_{L2}]_{10\times1} + [B_{L3}]_{1\times1}\right). \quad (39)$$

Including the previous equations in the extended SE requires determining the partial derivatives with respect to each input parameter evaluated at the operating point (P, Q and U). The derivative of the output with respect to the active power is:

$$\frac{\partial Qc}{\partial P} = \frac{\partial\left([W_{L3}]_{1\times10} \times [O_{L2}]_{10\times1} + [B_{L3}]_{1\times1}\right)}{\partial P} = \\ = [W_{L3}]_{1\times10} \times \frac{\partial\left([O_{L2}]_{10\times1}\right)}{\partial P} \quad (40)$$

The O_{L2} derivative is calculated with respect to the power by considering that $\text{tansig}'(x) = 1-\text{tansig}(x)^2$; therefore, the following applies:

$$\frac{\partial[O_{L2}]_{10\times1}}{\partial P} = \left([1]_{10\times1} - [O_{L2}]_{10\times1} \circ [O_{L2}]_{10\times1}\right) \circ \frac{\partial\left([W_{L2}]_{10\times5} \times [O_{L1}]_{5\times1}\right)}{\partial P} = \\ = \left([1]_{10\times1} - [O_{L2}]_{10\times1} \circ [O_{L2}]_{10\times1}\right) \circ \left([W_{L2}]_{10\times5} \times \frac{\partial\left([O_{L1}]_{5\times1}\right)}{\partial P}\right) \quad (41)$$

In addition, the derivative of the input layer with respect to power is given by:

$$\frac{\partial[O_{L1}]_{5\times1}}{\partial P} = \left([1]_{5\times1} - [O_{L1}]_{5\times1} \circ [O_{L1}]_{5\times1}\right) \circ \frac{\partial\left([W_{L1}]_{5\times3} \times [E_{L1}]_{3\times1}\right)}{\partial P} = \\ = \left([1]_{5\times1} - [O_{L1}]_{5\times1} \circ [O_{L1}]_{5\times1}\right) \circ \left([W_{L1,1}]_{5\times1} \times \frac{\partial\left(E_{L1(1,1)}\right)}{\partial P}\right) = \\ = \left([1]_{5\times1} - [O_{L1}]_{5\times1} \circ [O_{L1}]_{5\times1}\right) \circ [W_{L1,1}]_{5\times1} \quad (42)$$

where the operator $\circ$ corresponds to the Hadamard product.

B. BPNN training to model FSWT

The data values that a BPNN requires for training must include all of the possible running states for the system that will be modeled. Nevertheless, in an FSWT, certain capacitor banks are rarely used; to overcome this lack of data, a two-step process is proposed. The first relationship model is between the real component (Y_{Pi}) and the imaginary component (Y_{Qi}) of the complex apparent admittance of the asynchronous generator: $h(Y_{Pi},Y_{Qi}) = 0$. Thus, the effect of voltage in the reactive power demanded can be decoupled from the equation system. Usually, the machine parameters for h_{IGi} are not provided by manufacturers; under these conditions, to determine the relationship between Y_P and Y_Q, the use of measurement values is proposed. Therefore, for each P_i, Q_i and U_i measurement, the following equations can be written:

$$Y_{Pi} = \frac{P_i}{U_i^2} \\ Y_{Qi} = \frac{Q_i}{U_i^2} - Y_{C_i} \quad (43)$$

As a result, a set of Y_{Pi} and Y_{Qi} values can be obtained. Fig. 19 shows the function $h(Y_{Pi},Y_{Qi}) = 0$ for an Izar Bonus 1.3 MW when different capacitor bank steps are connected.

In the second step, $h(Y_{Pi},Y_{Qi}) = 0$ is used to obtain a training pattern for the BPNN that models the function $h_{e,IGi}(U_i,P_i,Q_i,Q_{Ci}) = 0$. Fig. 20 shows the training pattern for a BPNN used to model the behavior of the PFC for a Izar-Bonus 1.3 MW generator with four compensation steps at 187.5, 225, 262.5 and 350 kVAr. The BPNN training pattern has the input values P_i between 0 and P_n and U_i between 0.96 and 1.04 in pu. The resulting outputs are the Q_i and Q_{ci} values obtained using (23).

C. P and Q for WTGs at Sotavento Wind Park

In this section, these values are presented for each WTG model in the wind park (see Figs. 21–23); they are labeled from WT1 to WT24 (see Table 1).

References

[1] Handschin F, Scheweppe E. Static state estimation in electric power systems. Proc IEEE July 1974;62:972–83.
[2] Abur A. Power System State Estimation. Marcel Dekker Inc.; 2004.
[3] Niknam T, Firouzi B. A practical algorithm for distribution state estimation including renewable energy sources. Renew Energy 2009;34:2309–16.
[4] Feijoo A, Cidras J. Modeling of wind farms in the load flow analysis. IEEE Trans Power Syst 2000;15(1):110–5.
[5] Divya K, Nagendra Rao P. Models for wind turbine generating systems and their application in load flow studies. Elect Power Syst Res December 2005;76:844–56. Elsevier.
[6] Li Y, Luo Y, Zhang B, Mao C. A Modified Newton-Raphson power flow method considering wind Power. In: Asia-Pacific Power and Energy Engineering Conference. Wuhan: APPEEC; 2011.
[7] Castro L, Fuerte-Esquivel C, Tovar-Hernandez J. A unified aproach for the solution of power flows in electrical power systems including wind farms. Elect Power Syst Res 2011;81:1859–65.
[8] Guo-qiang S, Zhi-nong W, Bo P. Power system state estimation containing wind generators. In: Asia-Pacific Power and Energy Engineering Conference; 2009. APPEEC, art. no. 4918616, Wuhan.
[9] Cybenko G. "Approximation by superpositions of a sigmoidal function. Math Control Signals; 1989:303–14. Syst.2.
[10] Allen A. Probability, statistics, and queueing theory: with computer science applications. San Diego, California: Academic Press, Inc.; 1990.
[11] Peterson N, Adrian E, Aschmoneit F. State estimation with equality constraints. In: Tenth PICA Conference Proceedings, Toronto; May 1977. pp. 427–30.
[12] Wu F, Liu W, Lun S. Observability Analisis and Bad data processing for state estimation with Equality constraints. IEEE Trans Power Syst; February 1987. Winter Meeting, New Orleans, WM103-5.
[13] J. López, A. Dorado, J. Álvarez, A. Feijóo, C. Carrillo, J. Cidrás et al, The Sotavento Experimental Wind Park, in Póster, Global Windpower, París, 02-Abril-2002.
[14] E. Diaz-Dorado, C. Carrillo, J. Cidrás and E. Albo, Estimation of Energy Losses in a wind park, in Presentación, 9th Int. Conference EPQU'07, Barcelona, 9–11-Octubre-2007.
[15] www.sotaventogalicia.com, [Online].
[16] Díaz Dorado E, Carrillo C, Cidrás J. Control algorithm for coordinated reactive power compensation in a wind park. IEEE Trans Energy Convers 2008;23(4):1064–72.
[17] Werbos P. Beyond Regression: New Tools for Predicting and Analysis in the Behavioral Sciences. Ph. D. thesis. Hardvard University; 1974.
[18] Rumelhart D, Hinton GE, Williams R. Learning internal representations by error propagation. Parallel distributed processing: Explorations in the microstructure of cognition, vol. 1. Cambridge: The MIT Press; 1986. Foundations.
[19] Fukushima K, Miyake S, Ito T. Neocognitron: a neural network model for a Mechanism of Visual Pattern Recognition. MIT Press; 1989. pp. 526–34. Recopilado en Neurocomputing: foundations of Research, vol.
[20] Zarco Periñan P, Gomez Expósito A. Estimación de estado y de parámetros en redes eléctricas. Sevilla: Secretariado de publicaciones de la Universidad de Sevilla; 1999.